International Journal of Solids and Structures 48 (2011) 1370–1381

Contents lists available at ScienceDirect

International Journal of Solids and Structures

journal homepage: www.elsevier.com/locate/ijsolstr

A unified theory for cavity expansion in cohesive-frictional micromorphic media

Jidong Zhao *

Department of Civil and Environmental Engineering, Hong Kong University of Science and Technology, Clearwater Bay, Kowloon, Hong Kong

ARTICLE INFO

Article history:
Received 17 August 2010
Received in revised form 30 December 2010
Available online 25 January 2011

Keywords:
Cavity expansion
Micromorphic media
Strain-gradient plasticity
Microstructure
Size effect
Stress concentration

ABSTRACT

This paper presents a unified theory for both cylindrical and spherical cavity expansion problems in cohesive-frictional micromorphic media. A phenomenological strain-gradient plasticity model in conjunction with a generalized Mohr–Coulomb criterion is employed to characterize the elasto-plastic behavior of the material. To solve the resultant two-point boundary-value problem (BVP) of fourth-order homogeneous ordinary differential equation (ODE) for the governing equations which is not well-conditioned in certain cases, several numerical methods are developed and are compared in terms of robustness, efficiency and accuracy. Using one of the finite difference methods that shows overall better performance, both cylindrical and spherical cavity expansion problems in micromorphic media are solved. The influences of microstructural properties on the expansion response are clearly demonstrated. Size effect during the cavity expansion is captured. The proposed theory is also applied to a revisit of the classic problem of stress concentration around a cavity in a micromorphic medium subjected to isotropic tension at infinity, for which some conclusions made in early studies are revised. The proposed theory can be useful for the interpretation of indentation tests at small scales.

1. Introduction

The theory of spherical/cylindrical cavity expansion in finite or infinite media has been proved useful for a wide range of engineering applications. Bishop et al. (1945) and Hill (1950) were among the first who applied the theory to the prediction of indentation hardness of metals. In civil and geotechnical engineering, it has been commonly used in the interpretation of *in situ* tests, such as cone penetration tests (CPTs) and pressuremeter tests (PMTs) (Yu, 2000). In a typical theory of cavity expansion, it is assumed that the complex material behavior in either the indentation tests or the CPTs or PMTs can be simplified as a one-dimensionally expanded (or contracted) cavity. Closed-form solutions can be derived for the displacement and stress field around the cavity which can be used as convenient references for various engineering purposes.

Recent advances in instrument technologies make it possible now to apply indenter forces ranging from kilo-Newtons to pico-Newtons, and the measurable local displacements induced by indenter can reach the scale of microns or even nanometers. At such small scales, hardness tests have been found to show a strong Indentation Size Effect (ISE) when the dominant indentation deformation is comparable to the critical material characteristic length scale, e.g., at the order of tens of microns or even smaller (Fleck et al., 1994; Tabor, 1996; Nix and Gao, 1998; Gao et al., 1999; Gouldsone et al., 2007; Abu Al-Rub, 2007, and among others). Based on micro-indentation results, Nix and Gao (1998) have observed that the hardnesses of both single crystal copper and cold worked polycrystalline copper exhibit a similar nonlinear relation with the indentation depth which can be characterized by a reverse quadratic law. Huang et al. (2006) have observed that nano-indentation hardness data demonstrate an even stronger size effect which has to be explained by new hardness laws. Microstructural arrangements, such as Geometrically Necessary Dislocations (GNDs), have been found attributable to the observed ISE at small scales. The phenomenon of ISE cannot be properly explained by conventional theory of cavity expansion, since the existing theory has been developed within the framework of classic plasticity based on phenomenological continuum assumptions. There are no intrinsic material length scales in the theory that represent the typical size of important microstructures underpinning the material behavior at small scales such as in micro- or nano-indentations. To overcome the difficulty, appropriate modifications need to be made on conventional cavity expansion theory to include suitable terms that are reflective of the microstructural arrangements in the materials during indentation.

In this paper, we present a study to generalize the conventional theory of cavity expansion to account for the effect of microstructure. For this purpose, a special class of strain-gradient theory originally proposed by Mindlin (1964), later by Germain (1973) and more recently generalized by Fleck and Hutchinson (1997, 2001) and Chambon et al. (1998, 2001), is employed, wherein both the strains and strain gradients as well as their respective

* Tel.: +852 2358 8481; fax: +852 2358 1534.
E-mail address: Jzhao@ust.hk

0020-7683/$ - see front matter © 2011 Elsevier Ltd. All rights reserved.
doi:10.1016/j.ijsolstr.2011.01.023

work-conjugates are considered in formulating the constitutive relations. Along with introduction of gradient terms, one or more length scales are introduced which represents the typical dimension of the underlying microstructure in a continuum material. A material with deformable microstructures which can be so characterized is termed as "medium with microstructure" by Mindlin (1964) or "micromorphic medium" by Germain (1973) and Eringen (1999) (see also Georgiadis et al., 2000). To describe the yielding behavior for a wide range of materials, we further employ an extended form of Mohr–Coulomb criterion which involves both Cauchy stress and couple stress terms. As a result, the yield behavior of both frictional and cohesive materials can be characterized by the proposed theory.

Note that there have been a number of early studies on similar problems using non-conventional models, e.g., Eshel and Rosenfeld (1970), Cook and Weitsman (1966), Bleustein (1966). The attention in these studies, however, has predominantly been devoted to the investigation of the elastic stress/strain concentration at the surface of a cylindrical or spherical cavity in an unbounded medium. Some analytical studies have also been reported recently. For example, Gao (2003) has investigated the behavior of spherically expended shell using a gradient plasticity theory originally developed by Mühlhaus and Aifantis (1991) wherein higher-order spatial gradients of the effective plastic strain is considered in the yield condition. The more recent work by Gao et al. (2009) and Collin et al. (2009) have been limited to elasticity only. Zhao et al. (2007a) have conducted an elasto-plastic analysis on cylindrically expanded cavity using a Tresca-type criterion to describe the yield behavior. The present study is a generalization of this previous work.

2. Problem description

The cylindrical/spherical cavity is assumed to be expanded in a micromorphic medium. A strain-gradient theory based on that proposed by Mindlin (1964, 1965) and later extended by Germain (1973) is employed for the constitutive description (see also, Zhao et al., 2005, 2006, 2007a,b). Chambon et al. (1998, 2001) have employed a second-order strain-gradient model based on Germain (1973) to treat one-dimensional localization problems which bears certain similarity with the present cavity expansion problem.

The hollow cylinder/sphere is assumed to be initially subjected to a hydrostatic pressure p_0 both at the cavity surface and at the exterior surface, as shown in Fig. 1, and p_0 is sufficiently small so as not to cause any plastic deformation in the material. For the cylindrical case, a cylindrical polar coordinate system (r,θ,z) is adopted, whereas a spherical coordinate system (r,θ,φ) is used for the spherical case. Tension is taken as positive in this paper. From this initial state, the inner surface pressure is gradually increased from p_0 to p, which leads to an intermediate state as illustrated in Fig. 1. Upon loading, the hollow cylinder/sphere first experiences isotropic elastic deformation and then plastic yielding when the yield condition is met at any point in the hollow cylinder/sphere. Initial yielding is said to occur when any point in the cylinder/sphere first reaches the plastic state. The corresponding cavity pressure at this stage is called the initial yielding pressure and is denoted by p_{ci}. In Zhao et al. (2007a) it is found that initial yielding always occurs first at the inner wall surface for the cylindrical case. After this initial yielding stage, the cylinder is supposed to enter a partly plastic state which develops progressively with the increase of cavity pressure until the entire cylinder body becomes plastic. The pressure at which the entire body first enters the fully plastic state is called the critical yield pressure, and is denoted by p_{cf}. The spherical cavity expansion follows essentially the same process of initial yielding, plastic expansion and fully plastic yielding as the cylindrical case, as has been confirmed by the numerical calculation in the subsequent sections. We shall restrict our analysis up to the point of a fully plastic state. We assume the deformation remains infinitesimal. Indeed, as suggested by Hill (1950), for cylinders with the ratio of external and internal radii $n = b/a$ not too large (n less than 4 or 5, say) the strains and the displacement of the inner surface are relatively small so long as the fully plastic state has not reached. Prior to that state, the variation in a can be neglected when the stresses are computed.

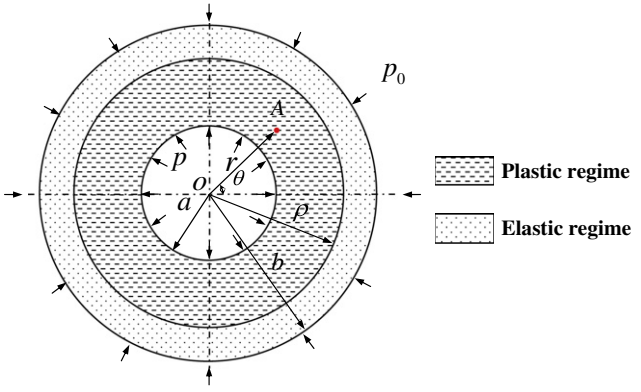

Fig. 1. Schematic of cylindrical/spherical cavity expansion in a cohesive-frictional medium.

2.1. Kinematics and constitutive description

In this subsection, we generalize the results in Zhao et al. (2007a) and Zhao and Pedroso (2008) and formulate the constitutive relations for both cylindrical and spherical cavity expansions in a unified manner. For the *cylindrical* case, a generalized plane strain condition as used in Zhao et al. (2007a) is assumed such that all the components for both strains and strain gradients associated with the z-coordinate vanish. The geometric axi-symmetry of the problem renders the displacement u at a material point A of the cylinder (see, Fig. 1) a function of r only. In consequence, the following non-zero components of strains and strain gradients can be expressed in terms of u (see also, Eq. (2) of Zhao et al., 2007a)[1]:

$$\left.\begin{aligned} &\epsilon_{rr} = u_{,r}, \quad \epsilon_{\theta\theta} = \tfrac{u}{r},\\ &\eta_{rrr} = u_{,rr}, \quad \eta_{\theta\theta r} = \tfrac{1}{r^2}(ru_{,r} - u),\\ &\eta_{r\theta\theta} = \eta_{\theta r\theta} = \tfrac{1}{r}\left(u_{,r} - \tfrac{u}{2r}\right) \end{aligned}\right\} \quad \text{(Cylindrical Cavity)}. \tag{1}$$

As for the *spherical* cavity expansion case, due to the geometric centro-symmetry of the problem, the displacement u at a material point A of the hollow sphere (see, Fig. 1) is also a function of r only. Following Zhao and Pedroso (2008), the non-zero components of strains and strain gradients, in this case, are ϵ_{rr}, $\epsilon_{\theta\theta}$, $\epsilon_{\varphi\varphi}$, η_{rrr}, $\eta_{\theta\theta r}$, $\eta_{\varphi\varphi r} = \eta_{\theta\theta r}$, $\eta_{\theta r\theta} = \eta_{r\theta\theta}$, $\eta_{\varphi r\varphi} = \eta_{r\varphi\varphi}$, and can be expressed in terms of u according to:

$$\left.\begin{aligned} &\epsilon_{rr} = u_{,r}, \quad \epsilon_{\theta\theta} = \epsilon_{\varphi\varphi} = \tfrac{u}{r},\\ &\eta_{rrr} = u_{,rr}, \quad \eta_{\theta\theta r} = \eta_{\varphi\varphi r} = \tfrac{1}{r^2}(ru_{,r} - u),\\ &\eta_{\theta r\theta} = \eta_{r\theta\theta} = \tfrac{1}{r^2}\left(ru_{,r} - \tfrac{u}{2}\right),\\ &\eta_{\varphi r\varphi} = \eta_{r\varphi\varphi} = \tfrac{1}{r^2}\left(ru_{,r} - \tfrac{u}{2}\right) \end{aligned}\right\} \quad \text{(Spherical Cavity)}. \tag{2}$$

[1] Even though the strain gradients are defined in a general tensorial form as $\eta_{ijk} = u_{k,\,ij}$, a direct partial differentiation with respect to the sub index can only be carried out in Cartesian coordinates, e.g., $\eta_{122} = u_{2,12}$. In case of cylindrical or spherical coordinates, it will work differently. For instance, $\eta_{r,\theta\theta} \neq u_{\theta,r\theta}$. In the current symmetric cylindrical cavity case, this results in that $\eta_{r\theta\theta} = \eta_{\theta r\theta} \neq \eta_{\theta\theta r}$. See Zhao and Pedroso (2008) for detailed derivations.

A generalized form of Hooke's law proposed in Mindlin (1964, 1965) is used here to describe the isotropic linear elastic behavior of the gradient-dependent solid (see also, Zhao et al., 2007a,b)

$$\left.\begin{aligned}\sigma_{ij} &= \lambda\epsilon_{kk}\delta_{ij} + 2\mu\epsilon_{ij},\\ \tau_{ijk} &= c_1\ell^2(\eta_{ipp}\delta_{jk} + \eta_{jpp}\delta_{ik}) + c_2\ell^2(\eta_{ppi}\delta_{jk} + 2\eta_{kpp}\delta_{ij} + \eta_{ppj}\delta_{ik})\\ &\quad + c_3\ell^2\eta_{ppk}\delta_{ij} + c_4\ell^2\eta_{ijk} + c_5\ell^2(\eta_{kji} + \eta_{kij})\end{aligned}\right\}. \tag{3}$$

where σ_{ij} and τ_{ijk} are the Cauchy stress and higher-order stress tensors, conjugate to the strain tensor and strain gradient tensor, respectively. λ and μ are the Lamé constants. c_i ($i = 1,5$) are elastic constants associated with gradient terms in a material. ℓ denotes an internal length scale resulted from the introduction of strain gradients, and is related closely to the dimension of microstructure in the material. For example, for single-/poly-crystal metallic materials ℓ has been related to the storage of Geometrically Necessary Dislocations. Its value can be estimated by fitting the predicted results of the constitutive prediction with measurable microstructural physical quantities from various micro-scale experiments such as micro-bending or micro-torsion tests. For example, ℓ has been identified by Nix and Gao (1998) in strain gradient plasticity as $\ell = (\mu/\sigma_y)^2 b$, where σ_y is a yield stress and b is the Burgers vector. For typical metallic materials ℓ is on the order of microns. It was emphasized by Fleck and Hutchinson (2001) that at least two distinct material length parameters need to be incorporated in any phenomenological gradient plasticity theory, with one relevant to problems where stretch gradients are dominant and the other applicable to cases where rotation gradients are important. For the cavity expansion problem being treated here, the rotation gradients vanish such that only one length scale ℓ is introduced which accounts for the effect of stretch gradients.

In consideration of Eqs. (1) and (2) and the general procedures provided by Zhao and Pedroso (2008) for deriving strain gradient relations in orthogonal curvilinear coordinates, we may readily obtain the following formulation of constitutive relations for the cylindrical cavity case in terms of the radial displacement:

$$\left.\begin{aligned}\sigma_{rr} &= (\lambda+2\mu)u_{,r} + \tfrac{\lambda}{r}u,\\ \sigma_{\theta\theta} &= \lambda u_{,r} + \tfrac{\lambda+2\mu}{r}u,\\ \sigma_{zz} &= \lambda\left(u_{,r} + \tfrac{u}{r}\right),\\ \tau_{rrr} &= c\ell^2\left(5u_{,rr} + \tfrac{4}{r}u_{,r} - \tfrac{13}{4r^2}u\right),\\ \tau_{r\theta\theta} &= \tau_{\theta r\theta} = c\ell^2\left(\tfrac{3}{4}u_{,rr} + \tfrac{11}{4r}u_{,r} - \tfrac{7}{4r^2}u\right),\\ \tau_{rzz} &= \tau_{zrz} = c\ell^2\left(\tfrac{3}{4}u_{,rr} + \tfrac{3}{4r}u_{,r} - \tfrac{1}{2r^2}u\right),\\ \tau_{\theta\theta r} &= c\ell^2\left(\tfrac{3}{2}u_{,rr} + \tfrac{7}{2r}u_{,r} - \tfrac{11}{4r^2}u\right),\\ \tau_{zzr} &= c\ell^2\left(\tfrac{3}{2}u_{,rr} + \tfrac{3}{2r}u_{,r} - \tfrac{5}{4r^2}u\right)\end{aligned}\right\} \quad \text{(Cylindrical Cavity)} \tag{4}$$

and the following form for the spherical cavity case:

$$\left.\begin{aligned}\sigma_{rr} &= (\lambda+2\mu)u_{,r} + \tfrac{2\lambda}{r}u,\\ \sigma_{\theta\theta} &= \sigma_{\varphi\varphi} = \lambda u_{,r} + \tfrac{\lambda+2\mu}{r}u,\\ \tau_{rrr} &= c\ell^2\left(5u_{,rr} + \tfrac{6}{r}u_{,r} - \tfrac{9}{2r^2}u\right),\\ \tau_{r\theta\theta} &= \tau_{\theta r\theta} = c\ell^2\left(\tfrac{3}{4}u_{,rr} + \tfrac{7}{2r}u_{,r} - \tfrac{9}{4r^2}u\right),\\ \tau_{r\varphi\varphi} &= \tau_{\varphi r\varphi} = c\ell^2\left(\tfrac{3}{4}u_{,rr} + \tfrac{7}{2r}u_{,r} - \tfrac{9}{4r^2}u\right),\\ \tau_{\theta\theta r} &= \tau_{\varphi\varphi r} = c\ell^2\left(\tfrac{3}{2}u_{,rr} + \tfrac{5}{r}u_{,r} - \tfrac{4}{r^2}u\right)\end{aligned}\right\} \quad \text{(Spherical Cavity)}. \tag{5}$$

Note that in both Eqs. (4) and (5) we have employed a single gradient-dependent elastic parameter c to replace the five c_i ($i = 1,5$) in Eq. (3) by setting $c = 2c_1 = 4c_2 = c_3 = c_4 = 2c_5$. In doing so, it is assumed that each individual strain gradient terms contributes equally to τ_{ijk} (see also, (Mindlin, 1965; Zhao et al., 2007a) for more information). c may be physically interpreted as a material parameter dependent on the hardness/shear resistance of important microstructures in a material. For example, for an inclusion problem, c may be taken to denote the bulk modulus of a soft or hard inclusion in the matrix. c/μ may be regarded as the stiffness ratio between the inclusion and the matrix in a material. Admittedly, further experimental evidence is required to justify this explanation. It is also interesting to note that Gao and Ma (2010a,b) have developed a first gradient elasticity theory of Helmholtz type, in which the gradient-dependent elastic parameters have been directly replaced by the conventional Lamé constants λ and μ. This is indeed similar to a special case of the current formulation that $c/\mu = 1$.

In the absence of body forces, the equilibrium equation for the radial direction of the cavity can be expressed in the following unified form for both cases:

$$\frac{d\sigma^*_{rr}}{dr} + \frac{k}{r}(\sigma^*_{rr} - \sigma^*_{\theta\theta}) = 0, \tag{6}$$

where $k = 1$ for the cylindrical case, and $k = 2$ for the spherical case. Clearly, the above unified form of equilibrium equation shows a similarity with the corresponding one in the conventional theory. As will be shown, based on Eq. (6), a unified numerical treatment for the cavity expansion problem in a hollow cylinder or a hollow sphere is possible. The generalized principal stresses in Eq. (6), σ^*_{rr} and $\sigma^*_{\theta\theta}$, respectively, take the following expressions:

$$\left.\begin{aligned}\sigma^*_{rr} &= \sigma_{rr} - \left(\tfrac{d\tau_{rrr}}{dr} + \tfrac{k}{r}(\tau_{rrr} - \tau_{\theta\theta r} - \tau_{r\theta\theta})\right),\\ \sigma^*_{\theta\theta} &= \sigma_{\theta\theta} - \left(\tfrac{d\tau_{\theta r\theta}}{dr} + \tfrac{1}{r}((k+1)\tau_{r\theta\theta} + \tau_{\theta\theta r})\right)\end{aligned}\right\}. \tag{7}$$

Note that the following symmetric properties hold for the higher-order stresses: $\tau_{r\theta\theta} = \tau_{\theta r\theta}$ for the cylindrical case, and $\tau_{r\theta\theta} = \tau_{\theta r\theta} = \tau_{r\varphi\varphi} = \tau_{\varphi r\varphi}$ for the spherical case.

As has been demonstrated in Zhao et al. (2007a), for the cylindrical case, the two generalized stresses, together with a third one:

$$\sigma^*_{zz} = \sigma_{zz} \tag{8}$$

are the only three non-zero stress components and have been treated as the generalized principal stresses. Similarly, for the spherical cavity case, it is readily verified, e.g., according to Zhao and Pedroso (2008), that the two generalized stress defined in Eq. (7) together with a third non-zero one $\sigma^*_{\varphi\varphi}$ which is identical with $\sigma^*_{\theta\theta}$:

$$\sigma^*_{\varphi\varphi} = \sigma^*_{\theta\theta}, \tag{9}$$

constitute the three non-zero generalized principal stresses.

The boundary conditions at the inner surface ($r = a$) and the outer surfaces ($r = b$) of the cylinder/sphere take the following form, respectively[2]:

$$\left.\begin{aligned}T_r(a) &= -\left(\sigma^*_{rr} + \tfrac{k}{r}\tau_{r\theta\theta}\right)\big|_{r=a} = p,\\ R_r(a) &= \tau_{rrr}|_{r=a} = 0,\\ T_r(b) &= \left(\sigma^*_{rr} + \tfrac{k}{r}\tau_{r\theta\theta}\right)\big|_{r=b} = -p_0,\\ R_r(b) &= \tau_{rrr}|_{r=b} = 0\end{aligned}\right\}, \tag{10}$$

where T_r and R_r are the surface traction and higher-order surface traction, respectively. Note that the boundary conditions in Eq. (10) have been chosen here to be consistent with the conventional cavity problem. In the presence of strain gradients and couple stresses, however, higher order surface tractions at both $r = a$ and $r = b$ may be important. They are neglected here merely for convenience. We also note that in the gradient plasticity approach following Mühlhaus and Aifantis (1991), such as in Gao (2003), one does not have to deal with non-conventional boundary conditions such

[2] Note that Eq. (15) in Page 4346 of Zhao et al. (2007a) was inadvertently misprinted where the correct expression for T_r at $r = a$ should be the first one in Eq. (10) here.

as the higher-order surface tractions mentioned here. In this connection, it has an obvious advantage over the strain gradient theory used in the current paper.

2.2. A generalized yield criterion for cohesive-frictional materials

We assume the material is elasto-perfectly plastic. While Tresca criterion has been widely used for metals, alternative yield criteria such as Mohr–Coulomb have long been used to describe the pressure-dependent yield behavior of cohesive-frictional materials. For the cavity expansion problem, as has been shown in Zhao et al. (2007a), when the cavity pressure is enough large, $\sigma^*_{\theta\theta}(=\sigma^*_{zz})$ and σ^*_{rr} in the cylindrical cavity become, respectively, the major and minor generalized stresses, whilst σ^*_{zz} remains the intermediate one. In the spherical cavity case, numerical computations have indicated that $\sigma^*_{\theta\theta}=\sigma^*_{\varphi\varphi}$ are the major generalized stresses, and σ^*_{rr} the minor stress (note that tension is taken positive here), when the cavity pressure is high enough. We hereby propose the following generalized Mohr–Coulomb criterion to describe the yielding behavior in these materials (c.f., Chadwick, 1959; Carter et al., 1986):

$$f = N\sigma^*_{\theta\theta} - \sigma^*_{rr} - \kappa\sqrt{N} = 0, \tag{11}$$

where

$$N = \frac{1+\sin\phi}{1-\sin\phi}$$

and ϕ is the frictional angle for a frictional material; $\kappa/2$ has a magnitude of cohesion of the material. The use of generalized stresses not only offers a compact form in expressing the Mohr–Coulomb yield criterion, but also renders it convenient for later numerical manipulation. Meanwhile, this approach can be adapted with ease to other yield criteria, such as the Drucker–Prager criterion which has long been used as a rounded approximation of the Mohr–Coulomb criterion (see, e.g. Papanastasiou and Durban, 1997; Zhao et al., 2007b). The same idea is applicable to a more general case when there are other non-zero components for the generalized stress tensor (see, e.g., Zhao and Pedroso, 2008, for expressions of generalized stresses in more general cases). If suitable hardening is further considered, e.g., by modifying the coefficients involved in the expression, Eq. (11) can be further used as a yield function in more advanced hardening/softening constitutive models. We emphasize that, however, there is no direct experimental evident yet at the stage that can be used to justify this specific form of yield criterion for a material, due partially to the difficulty in determining the material length scale in the first place. However, we believe that Eq. (11) can be verified if adequate experimental data are available in the future.

Furthermore, by assuming the frictional angle $\phi = 0$ such that $N = 1$, the expression in Eq. (11) can be easily simplified to the Tresca criterion which has been used in Zhao et al. (2007a)

$$f = \sigma^*_{\theta\theta} - \sigma^*_{rr} - \kappa = 0. \tag{12}$$

On the other hand, when the cohesion is set to zero ($\kappa = 0$), Eq. (11) can also been reduced to the following form suitable for the description of purely frictional materials:

$$f = N\sigma^*_{\theta\theta} - \sigma^*_{rr} = 0. \tag{13}$$

3. Solution procedures for the cavity expansion problem

3.1. Mathematical reformulation for elastic expansion

Using Eq. (7) in the equilibrium equation of (6) leads to:

$$\frac{d\sigma_{rr}}{dr} + \frac{k}{r}(\sigma_{rr}-\sigma_{\theta\theta}) - \frac{d^2\tau_{rrr}}{dr^2} + \frac{k}{r}\frac{d(\tau_{\theta\theta r}+2\tau_{r\theta\theta}-2\tau_{rrr})}{dr} + \frac{k}{r^2}(2k\tau_{r\theta\theta}+k\tau_{\theta\theta r}-(k-1)\tau_{rrr}) = 0. \tag{14}$$

At the stage of purely elastic expansion of the hollow cylinder/sphere, there is no material point yielding (the stresses satisfy that $f < 0$ in Eq. (11)), so that one can substitute the elastic relations in Eqs. (4) or (5) into Eq. (14) and arrive at the following general form of fourth-order ordinary differential equation in terms of the radial displacement u:

$$\begin{Bmatrix} \frac{dy_1}{dr} \\ \frac{dy_2}{dr} \\ \frac{dy_3}{dr} \\ \frac{dy_4}{dr} \end{Bmatrix} = \begin{bmatrix} 0 & 1 & 0 & 0 \\ 0 & 0 & 1 & 0 \\ 0 & 0 & 0 & 1 \\ A_1 & A_2 & A_3 & A_4 \end{bmatrix} \begin{Bmatrix} y_1 \\ y_2 \\ y_3 \\ y_4 \end{Bmatrix}, \tag{15}$$

where $y_1 = u$, $y_2 = u'$, $y_3 = u''$ and $y_4 = u'''$. The coefficients $A_i (i = 1,4)$ have the following expressions for the cylindrical and spherical cases, respectively:

$$\left.\begin{aligned} A_1 &= \tfrac{51}{20r^4} - \tfrac{\lambda+2\mu}{5cr^2\ell^2} \\ A_2 &= \tfrac{\lambda+2\mu}{5cr\ell^2} - \tfrac{51}{20r^3} \\ A_3 &= \tfrac{\lambda+2\mu}{5c\ell^2} + \tfrac{61}{20r^2} \\ A_4 &= -\tfrac{11}{5r} \end{aligned}\right\} \quad \text{(Cylindrical case)}, \tag{16}$$

$$\left.\begin{aligned} A_1 &= -\tfrac{2(\lambda+2\mu)}{5cr^2\ell^2} \\ A_2 &= \tfrac{7}{5r^3} + \tfrac{2(\lambda+2\mu)}{5cr\ell^2} \\ A_3 &= \tfrac{\lambda+2\mu}{5c\ell^2} + \tfrac{37}{10r^2} \\ A_4 &= -\tfrac{4}{r} \end{aligned}\right\} \quad \text{(Spherical case)}. \tag{17}$$

During any stage of the elastic expansion, the boundary conditions at the cavity surface and the outer surface, as expressed in Eq. (10), present the following form in terms of $y_i (i = 1,4)$:

$$\left.\begin{aligned} T_r(a) &= (w_1y_4 + w_2y_3 + w_3y_2 + w_4y_1)|_{r=a} = p, \\ R_r(a) &= (h_1y_3 + h_2y_2 + h_3y_1)|_{r=a} = 0 \end{aligned}\right\}, \tag{18}$$

$$\left.\begin{aligned} T_r(b) &= (q_1y_4 + q_2y_3 + q_3y_2 + q_4y_1)|_{r=b} = -p_0, \\ R_r(b) &= (h_1y_3 + h_2y_2 + h_3y_1)|_{r=b} = 0 \end{aligned}\right\}, \tag{19}$$

where the coefficients have the following expressions for the two cases:

$$\left.\begin{aligned} w_1 &= 5, & w_2 &= \tfrac{6}{a} \\ w_3 &= -\left(\tfrac{\lambda+2\mu}{c\ell^2} + \tfrac{49}{4a^2}\right), & w_4 &= \tfrac{19}{2a^3} - \tfrac{\lambda}{ac\ell^2} \\ q_1 &= -5, & q_2 &= \tfrac{-6}{b} \\ q_3 &= \tfrac{\lambda+2\mu}{c\ell^2} + \tfrac{49}{4b^2}, & q_4 &= \tfrac{\lambda}{bc\ell^2} - \tfrac{19}{2b^3} \\ h_1 &= 5, \quad h_2 = \tfrac{4}{r}, & h_3 &= -\tfrac{13}{4r^2} \end{aligned}\right\} \quad \text{(Cylindrical case)}, \tag{20}$$

$$\left.\begin{aligned} w_1 &= 5, & w_2 &= \tfrac{10}{a} \\ w_3 &= -\left(\tfrac{\lambda+2\mu}{c\ell^2} + \tfrac{45}{2a^2}\right), & w_4 &= \tfrac{17}{a^3} - \tfrac{2\lambda}{ac\ell^2} \\ q_1 &= -5, & q_2 &= \tfrac{-10}{b} \\ q_3 &= \tfrac{\lambda+2\mu}{c\ell^2} + \tfrac{49}{4b^2}, & q_4 &= \tfrac{2\lambda}{bc\ell^2} - \tfrac{17}{b^3} \\ h_1 &= 5, \quad h_2 = \tfrac{6}{r}, & h_3 &= -\tfrac{9}{2r^2} \end{aligned}\right\} \quad \text{(Spherical case)}. \tag{21}$$

Note that in the above equations, $h_i (i = 1,3)$ applies to both $r = a$ and $r = b$.

3.2. Conditioning of the boundary value problem

For purely elastic expansion, the governing equation in Eq. (15) together with the boundary conditions in (18) and (19) constitutes a homogeneous ordinary differential equation (ODE) system of two-point *boundary value problem* (BVP). While the exact analytical solution for such a complex problem is difficult to find, it can be solved numerically. A simple shooting method (SSM) in conjunction with an explicit Runge–Kutta (RK) method (4/5-th order with the Dormand–Prince pair) and the Broyden's iteration algorithm has been developed in Zhao et al. (2007a) to solve the cylindrical expansion problem. In solving the cylindrical expansion problem, the simple shooting method has shown a general stability and consistency. However, its solution with the gradient-dependent expansion problem is not without pitfalls. It has been found that, if very stringent tolerance is used for the solution of a thick-walled hollow cylinder or sphere, the numerical computation may encounter difficulty in achieving convergence. Note that the thick cylinder/sphere case can be of particular importance for many situations, e.g., a cavity expanded in unbounded media as an extreme case. This numerical issue is further aggregated when small values for the internal length scale (ℓ/a) and (/or) gradient-dependent modulus (c/μ) are used. A further investigation found that both the numerical scheme and the property of the ODE itself are attributable for the numerical breakdown. In order to understand the origin of the problem, it is helpful to look into the behavior of the ODE in (15).

First of all, it is well-known that the stability of a numerical approach for a boundary value problem depends crucially on the well-conditioning of the BVP. A "well-conditioned" boundary value problem implies that a small change in the coefficients of the ODE (e.g. Eqs. (16) and (17) here) or boundary conditions (e.g., Eq. (18) and/or Eq. (19) here) should produce only a small change in the solution. A stable and accurate numerical algorithm, if applied to solve such a BVP, should thus be able to produce accurate results as well. According to the theory of ordinary differential equation, e.g., Ascher et al. (1995), a *conditioning constant* (or *stability constant* in some other literature) can be used to measure the conditioning of a BVP. If the conditioning constant of a given problem is of moderate size, the problem is generally considered to be well-conditioned. In defining the conditions under which the conditioning constants can be bounded (by constants of moderated size), the concept of *dichotomy* has been developed based on a generalization of the IVP uniform stability notion. It has been proved that dichotomy, if it can be found, is not only sufficient but necessary for a BVP to be well-conditioned. To derive the conditioning constant and dichotomy, the first important step is to derive a Green's function which is related to the inverse of a differential operator to express the solution to a linear BVP. Construction of the Green's function for a BVP involves a linear mixed-order system of ODEs with corresponding linear boundary conditions. It is only possible when a complete set of solutions to the homogeneous problem is known which, however, is not always readily available in practice. It is therefore difficult to construct a Green's function for the analysis of its well-conditioning. The current problem falls precisely to this latter category. While we do not exclude the possibility that a Green's function and the dichotomy can be found for the current problem, further exploration on this topic is beyond the scope of this paper.

Nevertheless, a direct inspection of the ODE with its BCs can still yield useful information on the conditioning of the BVP which helps us seek possible improvements on the solution procedures. Firstly, a careful inspection of the solution by using the simple shooting method has found that, either in the case of very small values of $c\ell^2$, or the integration interval being very large, the system of linear equations in Eq. (15), with coefficients $A_i(i=1,4)$ defined in Eqs. (16) and (17), becomes extremely ill-conditioned. As is readily found, there is a term involving $c\ell^2$ in the denominator of all the expressions except A_4. When either c or ℓ or both is very small, this term become dominant in $A_i(i=1,3)$. This could cause numerical problems in the computation, in particular for y_4. Indeed, using the simple shooting method we have investigated the elastic expansion of a cylindrical cavity with a thickness of $n=b/a=4.0$. A set of different values for ℓ/a have been chosen for the investigation. It has been found that the overall behavior of $y_i(i=1,3)$ is not particularly sensitive to the change of ℓ/a. In all cases the variation of $y_i(i=1,3)$ with respect to r in the cylinder shows a monotonic curve with no dramatic change of curvature observed. In contrast, a quite different scenario has been observed for that of y_4. As is shown in Fig. 2, when a relatively large ℓ/a is used, i.e., $\ell/a=0.5$, 0.3 or 0.2 here, the overall curve follows a similar monotonic trend as that of $y_i(i=1,3)$. However, when ℓ/a becomes smaller, i.e., $\ell/a=0.15$, 0.125 or 0.1, an obvious turning point in curvature is found at around $r/a=1.15$ and the curvature becomes even sharper with a further smaller value of ℓ/a. We have also found that if a value of ℓ/a smaller than 0.1 is used with all the other conditions the same, the numerical shooting method fails to converge at all. The same observation has been found with regard to the gradient-dependent stiffness parameter c and the integration interval $(b-a)$ or $n=b/a$. Since in the simple shooting method we have to evaluate the derivatives of the solution, either by differential quotient or difference quotient, and therefore an inversion of an auxiliary matrix, a warning was reported that the matrix is close to singular or badly scaled with an estimate of condition number (*RCON*) close to 5.5×10^{-36}. Numerical experience tells us there might be two solutions of the ODE that decay very fast (i.e., exponentially) as r increases which cannot be distinguished numerically by their values at $r=b$. The linear system for their coefficients in the linear combination that forms the solution of the BVP is numerically singular. There may be also a third solution which decays very fast (i.e., exponentially again) as r increases, leading to an ill-conditioned linear system if b or n is large and the boundary condition involves the value of this solution at $r=a$. The situation will become hopelessly bad if we wish to deal with the case of infinite media where $b\to+\infty$.

Another factor attributable to the numerical breakdown of the simple shooting method in solving the thick-wall cavity expansion problems is the inaccurate initial guess at the starting end (e.g., $r=a$) and the resultant error accumulated and magnified over the long span of the shooting interval. As mentioned earlier, we need to make an initial guess for some unknowns at one end

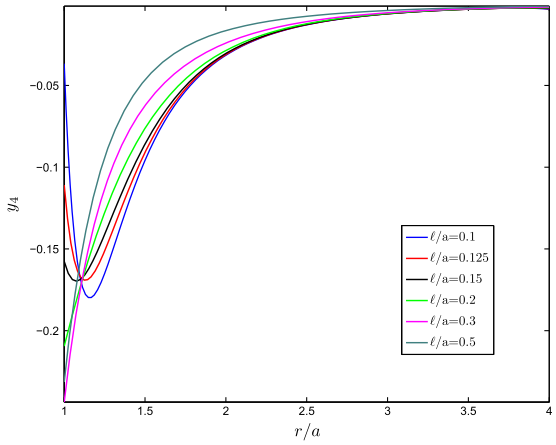

Fig. 2. Sensitivity of the solution of $y_4(=u''')$ to ℓ/a in elastic expansion. Six sets of ℓ/a were chosen: $\ell/a=0.1$, 0.125, 0.15, 0.2, 0.3, 0.5. Other material parameters used are: $a=1.0$, $b/a=4.0$, $\lambda/\mu=2.0$, $p_0/\mu=0.1$, $c/\mu=1.0$, $\kappa/p_0=3.0$, $\phi=30^\circ$, $tol=10^{-5}$.

(i.e., y_3 and y_4 at $r = a$) upon which the stability of simple shooting method depends crucially. Sometimes even a slight deviation involved in the initial guess with respect to the exact values could result in greatly magnified errors at the other end, which prevents the solution to converge. The greater the integration range (i.e., $(b - a)$ or $n = b/a$ here) is, the worse the situation will become. If large range of integration is combined with small value of length scale ℓ or c, the simple shooting quickly fails to work. Meanwhile, as is known, one-step methods such as high-order Runge–Kutta methods are sensitive to the step size. The use of very small step size could also lead to excessive roundoff errors and cause possible divergence of the solution, which could contribute to the failure of the simple shooting method in solving problems with large intervals as well.

3.3. Robust solution procedures

We have hereby developed three new approaches in attempting to solve the cavity expansion problems effectively. The first of such is a multiple shooting method (MSM). In view of the fact that the simple shooting method has worked perfectly when the integration interval is tight (i.e., thin wall case), we may divide the entire integration span into a number of small subintervals, and apply the simple shooting method over each subinterval. Constraints of continuation are imposed at the boundary of two neighboring subintervals. In this way we wish to reduce the possible cumulative errors caused by inaccurate initial guess. Meanwhile, suitable refinement of subdivision can be purposely chosen in the neighborhood of points where dramatic curvature changes are expected to occur in the solution, i.e., $r = 1.15a$ for y_4 as shown in Fig. 2. In this way, it is expected that the well-conditionedness of the BVP at each local subinterval can be improved over the original single-interval case, as is the overall stability of the numerical solution. The multiple shooting algorithm developed here closely follows that proposed in Kelly (1968) and outlined in Ascher et al. (1995) and Stoer and Bulirsch (2000). Detailed formulations and algorithm of the multiple shooting method will not be presented here.[3]

In addition, we have also developed two finite difference methods for the present problem. The finite difference methods are based on a C^1 piecewise cubic polynomial and an implicit Runge–Kutta formula with a continuous extension. The first of the two is based on those developed in Kierzenka and Shampine (2001). For a mesh similar like that used in the multiple shooting method, $a = x_0 < x_1 < \cdots < x_m = b$, the method can be considered as a collocation with a piecewise function $\mathbf{S}(\mathbf{x})$ for the function to be integrated, i.e., the right-hand side of Eq. (15). $\mathbf{S}(\mathbf{x})$ satisfies the boundary conditions and for each subinterval $[x_i, x_{i+1}]$ of the mesh it is a cubic polynomial that collocates at the ends of the subinterval and the midpoint. It is continuous at the endpoints of each subinterval and has a C^1 continuity within this subinterval. The collocation method can be regarded equivalent to the 3-stage Lobatto IIIa implicit Runge–Kutta formula which was termed in Kierzenka and Shampine (2001) as the *Simpson method*. In tackling the practical difficulty with finite difference and collocation methods in finding a mesh for which the asymptotic arguments that justify error estimation and mesh selection are valid, a formulation based on control of the residual through analytical condensation of the implicit Runge–Kutta formula originally proposed in Enright and Muir (1993) was implemented. The residual is zero at both ends. At the midpoint, its value is used to measure the extent the algebraic equations define the method. In computing the finite difference approximation to the Jacobians matrix, the algorithms developed by Shampine and Reichelt (1997) is employed. To enhance the global convergence of the simplified Newton iteration when guesses for a mesh and solution are poor, a weak line search is used for an affine-invariant convergence test. However, if the Newton iterations converge slowly, a more efficient way is to stop iterating at all and redistribute the mesh. Instead of following the popular way of mesh selection by redistributing mesh points with a global strategy based on inverse interpolation which has been proved unsatisfactory when the mesh is crude and the function to be integrated is only piecewise smooth, a local strategy is followed by adding equally spaced mesh points to a subinterval for which the residual is greater than the tolerance. This method has been implemented into the recent release of MATLAB, termed as *BVP4C*, and has been examined in solving our problem.

The second finite difference method is based on a newer package called *BVP6C* recently developed by Hale and Moore (2008) based on the residual control framework of *BVP4C*. In the new package, a sixth-order solver, MIRK4, is adopted instead of the fourth-order one used in the original *BVP4C* for the interpolant. The norm of the residual on each subinterval is computed by the 7-point Lobatto quadrature method. In Hale and Moore (2008) it has been demonstrated that *BVP6C* is more accurate and efficient than the original *BVP4C*. Its performance in solving our cavity expansion problem will be examined in this paper in close comparison with other methods mentioned above.

The performance of the four methods has been compared, in terms of their consistency, stability and efficiency in solving the cavity expansion problem. Overall, both BVP4C and BVP6C demonstrate better robustness and consistency than the two shooting methods. This is especially true when the tolerance is tightened to a much stringent level of $tol = 10^{-15}$. It is also found that BVP4C and BVP6C have also shown greater efficiency in terms of CPU time than the shooting methods in solving the present problem. In solving thick-walled problems with a small length scale, when greater thickness ratio $n = b/a$ is used, both SSM and MSM fail to converge. In contrast, the two finite difference methods, BVP4C and BVP6C, are particularly robust and can work well when b/a is increased as large as 500. BVP4C and BVP6C also outperform the two shooting methods when the sensitivity to the range of ℓ/a is examined.

3.4. Load stepping and elasto-plastic expansion

Numerical calculations confirm that, during both cylindrical and spherical cavity expansion, when the cavity pressure is high enough, $\sigma^*_{\theta\theta}$ and σ^*_{rr}, respectively, become the maximum and minimum generalized stresses. Moreover, the initial yielding is always found to occur at the cavity surface, with the yielding governed by Eq. (11). Further loading will cause the plastic zone in the hollow cylinder or sphere to develop progressively from the inner cavity surface towards the exterior surface. Accordingly, the numerical load stepping procedure outlined in Zhao et al. (2007a) for both elastic and elasto-plastic expansion stages can be followed, and any of the four methods in last subsection can be used in the procedure. Specifically, from the initial state to the initial yielding, we gradually increase the internal cavity pressure and calculate the resultant stress and displacement field in the sphere/cylinder, and check if the initial yielding condition is satisfied. Once the cylinder/sphere enters initial yielding, the numerical calculation will be switched from a purely elastic expansion to a plastic expansion stage. At the plastic expansion state, we shall cease to use the internal pressure as the driving variable, but employ the plastic radius ρ (see Fig. 1) as a known condition for each sub-increment.[4]

[3] Interested readers may contact the author to request a copy of the MATLAB source code.

[4] It is equivalent that force control is applied to the elastic expansion stage but displacement control is used for the plastic expansion.

With ρ being increased from the inner surface a to the external surface b under suitably chosen small step size, the numerical computation advances until the fully plastic stage is reached ($\rho = b$). At the end of each sub-increment of ρ, the internal pressure and outer wall displacement will be computed.

The displacement and the stress fields can be accurately determined for the entire elastic expansion stage up to the initial yielding (inclusive). Once initial yielding occurs and the hollow cylinder/sphere enters partly/fully plastic expansion stage, plastic flow rule has to be introduced in order for the deformation/stress field to be completely determined. As we only wish to determine the stress field and thereby the pressure-expansion curve, the excessive complication caused by using the flow rule can be avoided by developing iterative numerical approximation for the plastic expansion. A similar procedure for partly plastic expansion to that developed in Zhao et al. (2007a) is followed in this paper. The basic idea is to solve the elastic regime using any of the methods discussed in Section 3.3, albeit with different boundary conditions at the elastic–plastic boundary $r = \rho$. The new boundary conditions at $r = \rho$ satisfy the governing equation and the elastic Hooke's law (and therefore Eq. (15)), and at the same time satisfy the yield condition Eq. (11). As discussed in Zhao et al. (2007a), there will be one more unknown in this case such that iterative procedures have to be developed to reach a converged solution. Once the elastic regime solution is obtained, the cavity pressure is estimated through the traction boundary condition at the inner cavity wall, e.g., via Eq. (30) of Zhao et al. (2007a). An illustrative flow chart for the load stepping of elasto-plastic expansion is presented in Fig. 3.

In solving the plastic expansion problem with extreme parameter combinations, while both BVP4C and BVP6C excel the two shooting methods in almost all cases, we have also identified some special cases that differentiate BVP6C from BVP4C too. In some extreme cases, BVP4C may encounter issues of singular Jacobian when solving the collocation equations, whilst BVP6C works without difficulty. In consideration of the overall performance, BVP6C will be used in all calculations subsequently.

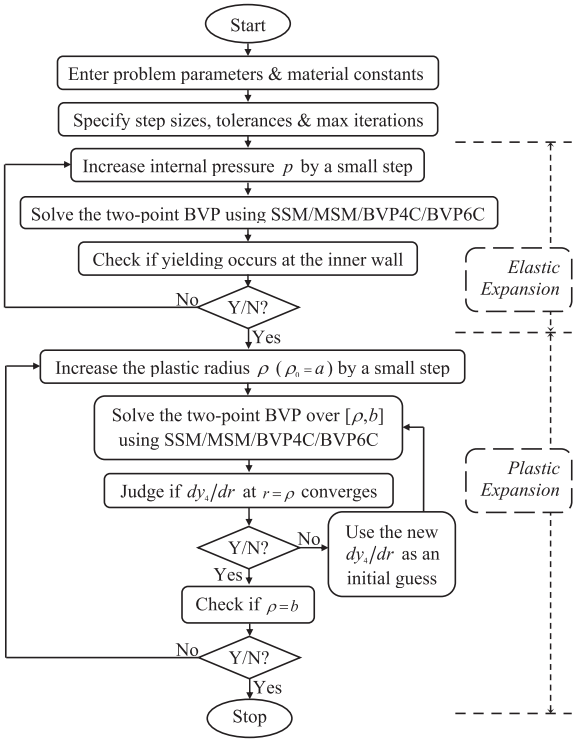

Fig. 3. Flow chart for the load stepping of elastoplastic cavity expansion.

4. Applications

4.1. Stress concentration at a cavity in an isotropic tension field

The stress concentration of a cavity in an isotropic tension field is a classical problem. In conventional theory, the stress concentration factor (SCF in brief in the sequel), in terms of the ratio between the hoop stress at the cavity surface and the far-field tension pressure, has been known to be 1.5 for the spherical case and 2.0 for the cylindrical case, respectively. The same problem has also been investigated in the past by non-classical theories. Eshel and Rosenfeld (1970), for example, have employed Mindlin's first-order strain-gradient theory (Mindlin, 1964) to investigate the stress concentration factor at the surface of a cylindrical hole under uniaxial tension. Cook and Weitsman (1966) have studied the elastic stress field due to a spherical inclusion or cavity in an infinite domain subjected to spherically symmetric tension at infinity. Using a strain-gradient theory, they demonstrated that the effect of stress concentration around the surface is much more remarkable than that observed by conventional theories. In a similar analysis using Mindlin's first-order strain-gradient theory, Bleustein (1966) found the stress concentration factor is larger than the value of 3/2 as predicted by classical elasticity. It was also found that a critical ratio between the cavity radius and the internal length scale, a/ℓ, exists, at which the stress concentration factor reaches a maximum. Note also that these early studies have also been limited to the *linear elastic* regime of the deformation.

A revisit of this classical problem is made here for two reasons. Firstly, these early studies often involve too many gradient-dependent material parameters which prevents the effect of strain gradients on the stress concentration from being clearly demonstrated and interpreted. In this paper we shall only use two gradient-dependent parameters, c and ℓ, for that purpose. In addition, we found that in all these early studies, the stress concentration has been computed in terms of the conventional hoop stress ($\sigma_{\theta\theta}$) only. However, the stress concentration reflects the overall mechanical response of the material at the cavity surface, and should be expressed by a comprehensive stress term that involves both conventional and higher-order stresses. In this connection, it is convenient to demonstrate the overall stress concentration effect using the generalized stress $\sigma^*_{\theta\theta}$ as defined in Eq. (7).

The formulation and the numerical solution procedure outlined in the previous sections have been employed to treat the problem again. It is assumed that the boundary at infinity is subjected to an isotropic tension pressure p_0. To approximate an infinite domain, a value of 100 for $n = b/a$ has been adopted. The values of other model parameters used in the computation are: $a = 1.0$, $\lambda/\mu = 2.0$, $tol = 10^{-10}$. ℓ/a has been chosen to be in a range between 10^{-3} to 1.0, along with five values for c/μ: 0.1, 0.5, 1.0, 2.0 and 5.0. Since only purely elastic computation is needed, there is no need to specify the parameters related to the yield criterion. By using the better-performed finite difference method, BVP6C, the stress concentration factor at the surface of a cavity in unbounded mircomorphic media has been calculated for both the spherical and cylindrical cases. The results are presented in Fig. 4 where both $\sigma_{\theta\theta}/p_0$ and $\sigma^*_{\theta\theta}/p_0$ are comparatively shown. Note that in the figure, the horizontal axis is drawn in logarithmic scale.

It can be observed from Fig. 4 that the stress concentration factors vary markedly with the length scale ℓ and the gradient-dependent stiffness parameter c. For the *spherical cavity case*, $\sigma^*_{\theta\theta}/p_0$ is larger than the conventional value 1.5 in all cases. Generally, a small value of ℓ/a with a bigger c/μ will lead to an observable difference between the predictions by the conventional theory and the micromorphic theory. However,when both c/μ and ℓ/a become small, the gradient effect diminishes quickly and the predicted gradient-dependent curves approach the conventional horizontal

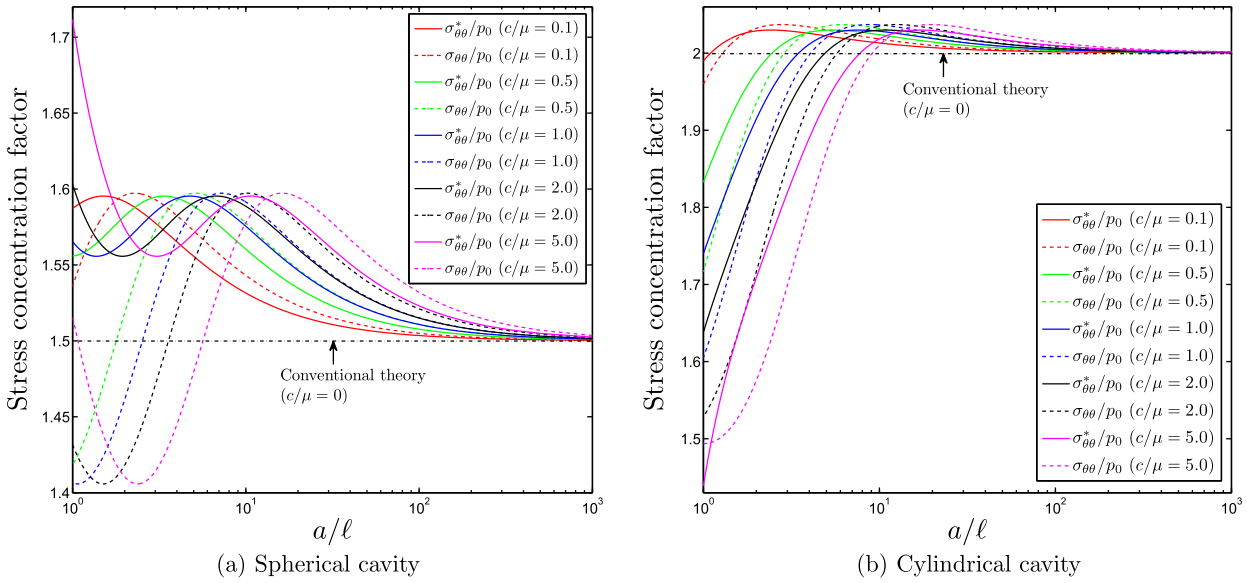

Fig. 4. Variation of the stress concentration factors (SCFs) in terms of normalized hoop stress ($\sigma_{\theta\theta}/p_0$) and generalized hoop stress ($\sigma^*_{\theta\theta}/p_0$) with c/μ and a/ℓ at a cavity in an infinite field subject to isotropic tension. (a) Spherical case; (b) cylindrical case. Other parameters used: $a = 1.0$, $\lambda/\mu = 2.0$, $tol = 10^{-10}$. $n = b/a = 100$ has been used to approximate the unbounded medium.

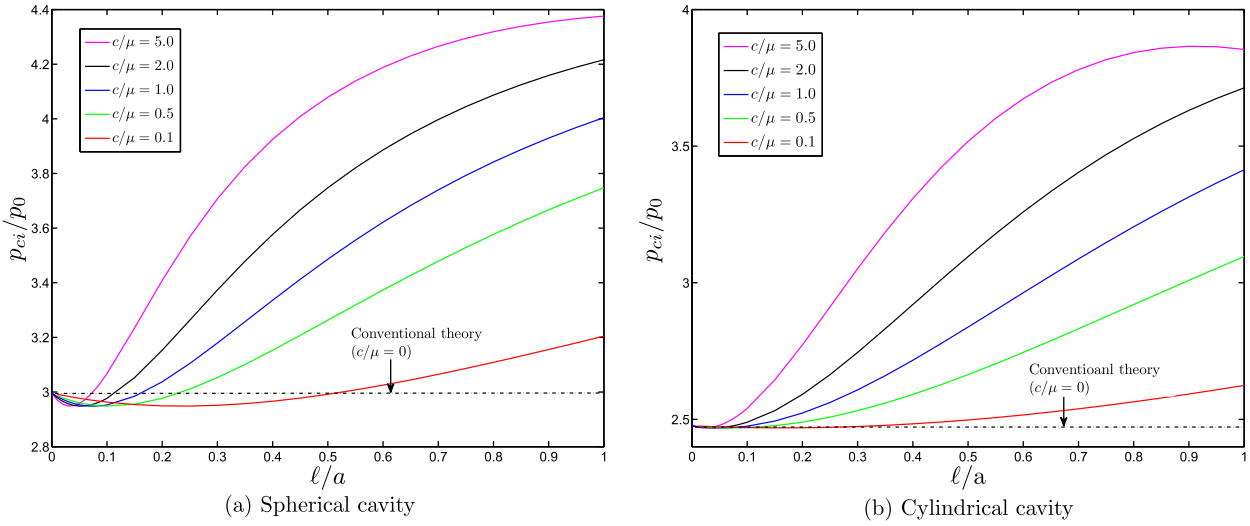

Fig. 5. Variation of normalized initial yield pressure (p_{ci}/p_0) with c/μ and a/ℓ for an internally pressured cavity. (a) Spherical case (conventional theory: $p_{ci}/p_0 = 2.994$ shown as the horizontal dash-dotted line); (b) cylindrical case (conventional theory: $p_{ci}/p_0 = 2.477$ shown as the horizontal dash-dotted line).

dotted line asymptotically. In the current parameter selection, it is also observed that the stress concentration factor in terms of $\sigma_{\theta\theta}/p_0$ will not alway be greater than 1.5. Its variation with c/μ and ℓ/a exhibits an interesting sinusoid-like trend with part of the curve below the horizontal dotted line of the classic theory. It is noteworthy that some past studies, i.e., Bleustein (1966), have claimed that the gradient-dependent SCF using $\sigma_{\theta\theta}/p_0$ is always greater than the classic one. The validity of this conclusion for a more general case, however, is questionable. As is shown here, the strain gradients might not necessarily always cause a stronger response. This is more evident in the *cylindrical cavity case* as shown in Fig. 4(b). In this figure, the horizontal broken line denotes results for the classic case where SCF = 2.0. As is shown, when ℓ/a is small (say smaller than 0.1), all gradient-dependent SCFs are greater than 2.0 and asymptotically approach the classical value when ℓ/a becomes vanishingly small. When ℓ/a becomes large, i.e., greater than 0.4 in the case of $c/\mu = 5.0$, both $\sigma^*_{\theta\theta}/p_0$ and $\sigma_{\theta\theta}/p_0$ demonstrate a smaller value than 2.0. The difference between the gradient case and the classic one can be as large as 25%.

Meanwhile, for the spherical cavity case, Bleustein (1966) mentioned that there is a critical ratio between a and ℓ, at which the SCF attains a maximum. We would, however, draw a different conclusion after an inspection of Fig. 4(a), from which we can see that the SCF could be even bigger with a steady decreasing in value of a/ℓ less than 1. There is only a *local* maximum for SCF existing when a/ℓ is between 1 and 20. However, for the cylindrical case, it is possible to have a critical ratio of a/ℓ for SCF to attain a *global* maximum, which is observable from Fig. 4(b).

4.2. Expansion of an internally pressured hollow sphere

The cavity expansion of an internally pressured hollow cylinder/sphere has also been investigated using the cavity expansion theory outlined in the preceding sections.

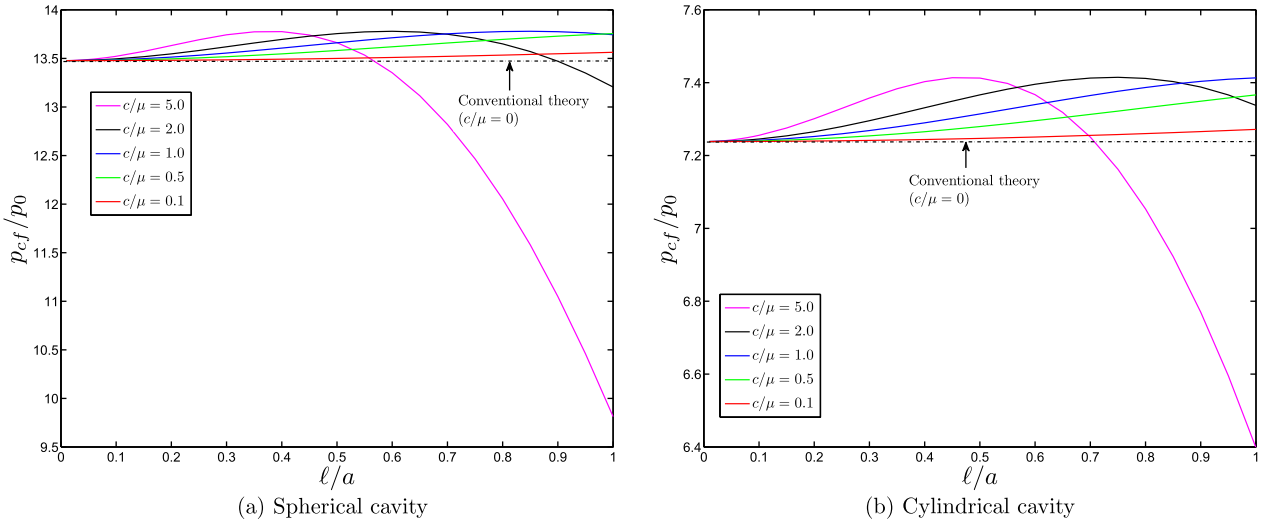

Fig. 6. Variation of normalized critical pressure at fully plastic yielding (p_{cf}/p_0) with c/μ and a/ℓ for an internally pressured cavity. (a) Spherical case (conventional theory $p_{cf}/p_0 = 13.477$ shown as the horizontal dash-dotted line); (b) cylindrical case (conventional theory: $p_{cf}/p_0 = 7.238$ shown as the horizontal dash-dotted line).

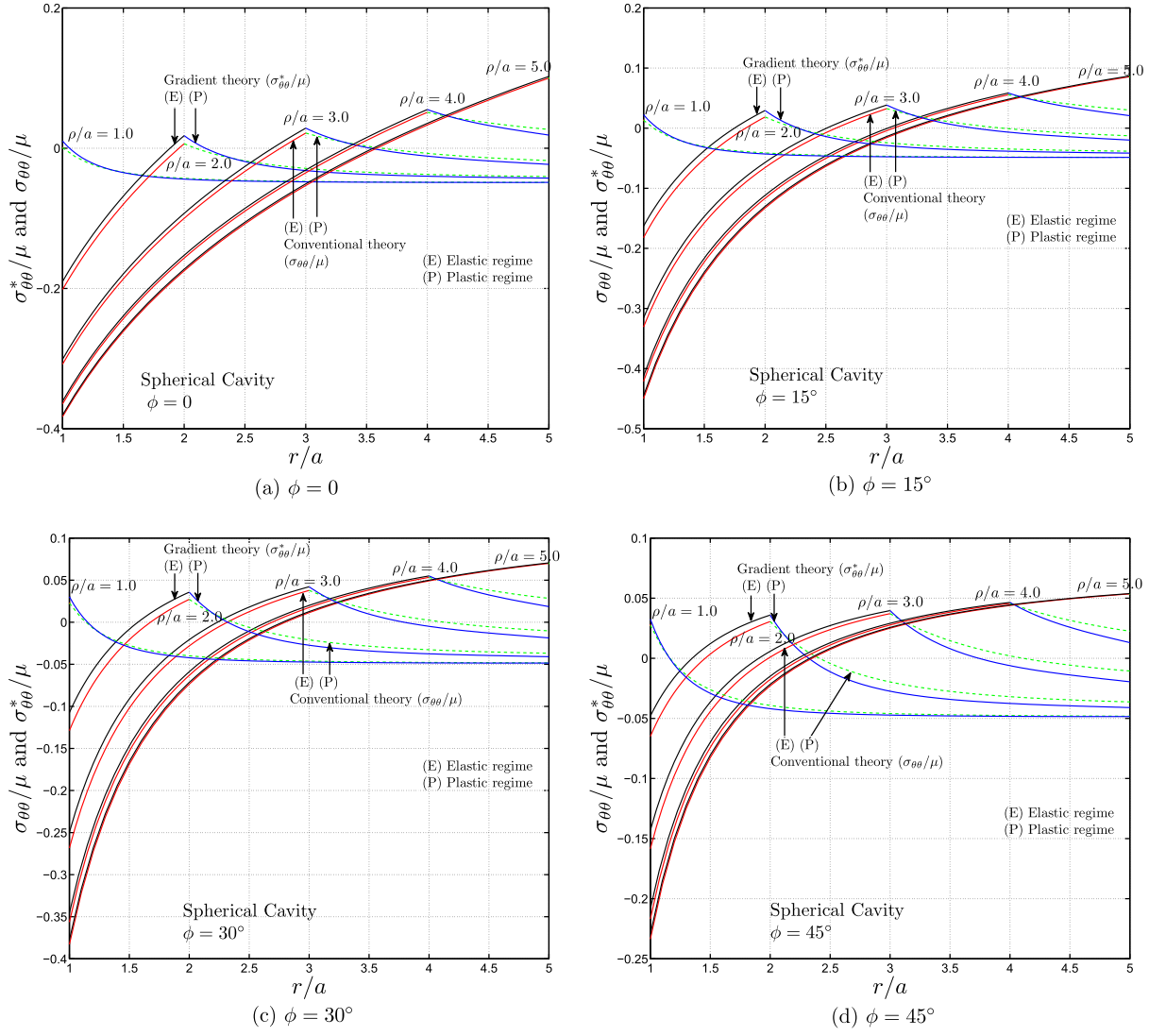

Fig. 7. Distribution of normalized circumferential stresses along the shell wall of an internally pressured spherical cavity at various plastic radii (ρ/a) for frictional-cohesive materials with different frictional angle. Conventional theory: $\sigma_{\theta\theta}/\mu$ (curves in red and in green); gradient theory: $\sigma^*_{\theta\theta}/\mu$ (curves in black and in blue). (a) $\phi = 0$; (b) $\phi = 15°$; (c)$\phi = 30°$; (d)$\phi = 45°$. (For interpretation of the references to colour in this figure legend, the reader is referred to the web version of this article.)

4.2.1. Initial yielding and fully plastic yielding

The plastic yielding of an internally pressured tube/shell has also been investigated. Figs. 5 and 6 display the variation of normalized initial yield pressure and the critical pressure at full plastic state, respectively, of an internally pressured tube/shell with different c and ℓ. For both figures, the following parameters have been used: $a = 1.0$, $\lambda/\mu = 2.0$, $\phi = 0$, $tol = 10^{-10}$, $n = b/a = 8.0$, $m = 1000$, and a value of 200 for N_ρ is adopted to ensure the convergence for calculation of dy_4/dr at the elastic plastic boundary $r = \rho$. As is shown in Fig. 5, for both the cylindrical and spherical cases, with the increase of ℓ from 0 to a, the curve of p_{ci} first attains a minimum slightly smaller than the conventional value (broken line) before rising above and becomes much higher at $\ell = a$. The trend is particularly obvious in case of large c. For the spherical cavity case, it is noticed that for $c/\mu = 0.1$ and $\ell = a$, the initial yield pressure is around 6% higher than the conventional value. If large c is used, i.e. $c/\mu = 5.0$, the increase in p_{ci}, as compared to the conventional value, can reach as much as 46%. Similar observations can be found for the cylindrical case. While it is obvious that the increase in microstructural length and gradient-dependent stiffness in general helps us to achieve a higher initial yield pressure, it is different for the critical pressure at full plastic stage. As is seen from Fig. 6, certain selections of ℓ and c may help p_{cf} achieve a small peak above the (broken) line of conventional value (the increase is not significant and is normally less than 3%). Further increase of c, however, could result in a significant decrease in p_{cf}. In the case of $c/\mu = 5.0$ and $\ell = a$, the decrease in p_{cf} as compared to the conventional value is around 27% for the spherical case and 11.6%. Note that these observations are consistent with our findings in a previous paper (Zhao et al., 2007a).

4.2.2. Stress distribution during plastic expansion and the effect of friction

It is also interesting to see the stress distribution during the plastic expansion of the cavity. To avoid excessive repeat, we only present the results for the spherical cavity case as the cylindrical case is quite similar. The following parameters have been used in the calculation: $a = 1.0$, $n = b/a = 5$, $\lambda/\mu = 2.5$, $\ell/a = 0.2$, $c/\mu = 5.0$, $p_0/\mu = 0.05$, $\kappa/p_0 = 3.0$, $tol = 10^{-10}$, $N_\rho = 200$. Four different frictional angles, $\phi = 0$, 15°, 30° and 45°, have been used to investigate the

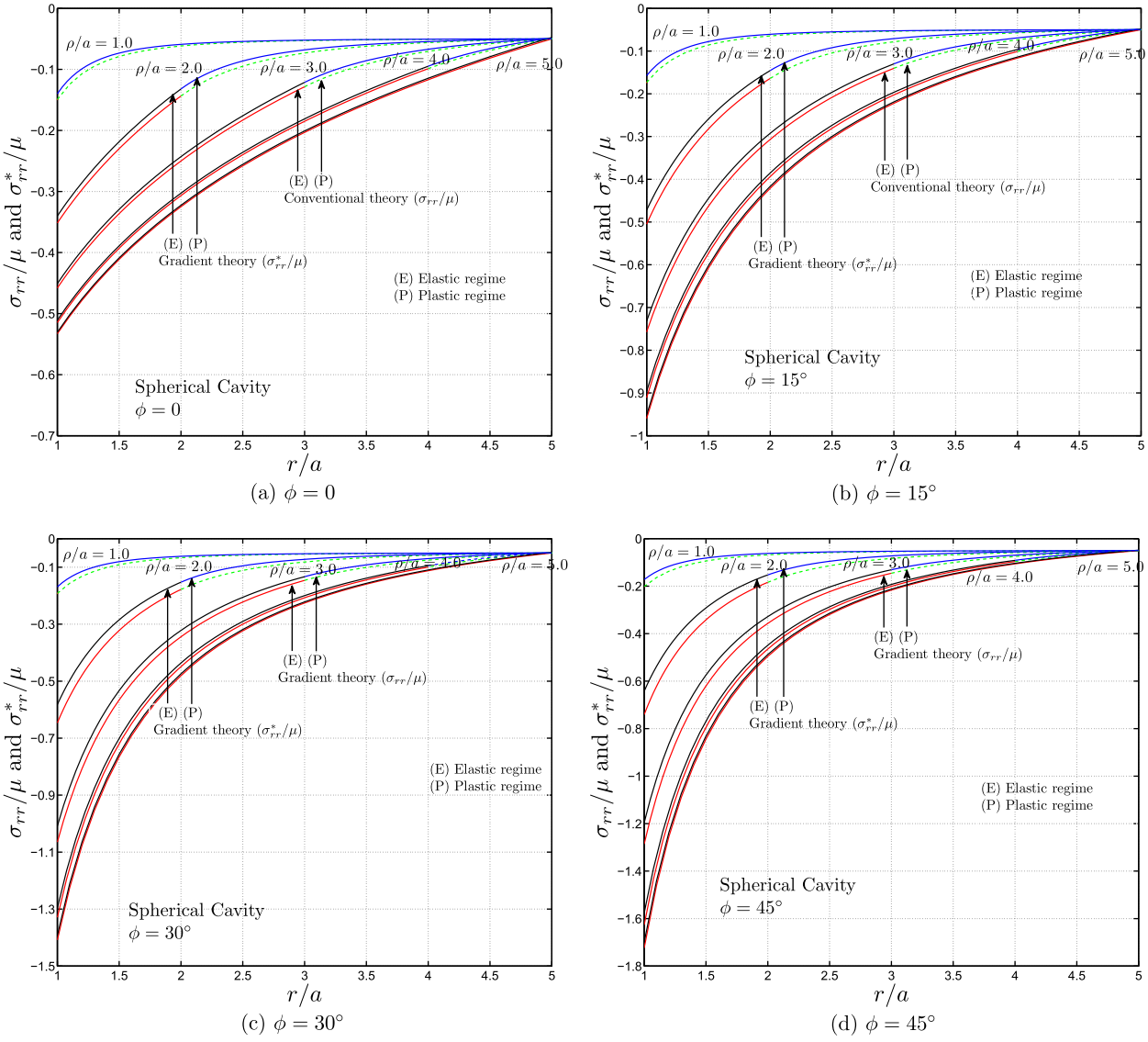

Fig. 8. Distribution of normalized radial stresses along the shell wall of an internally pressured spherical cavity at various plastic radii (ρ/a) for frictional-cohesive materials with different frictional angle. Conventional theory: σ_{rr}/μ (curves in red and in green); gradient theory: σ^*_{rr}/μ (curves in black and in blue). (a) $\phi = 0$; (b) $\phi = 15°$; (c) $\phi = 30°$; (d) $\phi = 45°$. (For interpretation of the references to colour in this figure legend, the reader is referred to the web version of this article.)

effect of friction. Figs. 7 and 8 depict the distribution of generalized major and minor principal stresses in the hollow sphere during the expansion of the cavity at different values of plastic radius ρ.

From Fig. 7 one can see that the frictional angle has an appreciable influence on the stress distribution in the sphere wall. It appears that when the frictional angle ϕ is at 15° and 30°, the gradient-dependent generalized stress $\sigma^*_{\theta\theta}$ is slightly more inhomogeneous than the rest cases, which is a consistent trend with the conventional stress. Compared to the conventional theory, it is observed that in the plastic regime, the gradient-dependent generalized stress $\sigma^*_{\theta\theta}$ is always above the conventional stress. The trend continues in the elastic regime only in a very small region close to the plastic radius. The gradient-dependent stress becomes smaller than the conventional one at locations close to the external surface of the hollow sphere. We also see that the gradient theory can achieve a higher peak stress than the conventional theory at the boundary of elastic and plastic regimes. This peak value will increase steadily as the plastic radius moves towards the exterior sphere wall. As for the minor generalized stress σ^*_{rr}, we observe from Fig. 8 that the increase in frictional angle generally makes the radial stresses more compressive. The gradient-dependent stress curves, in all cases, lie above the conventional ones. Appreciable difference between the predictions by the two theories can be observed at the cavity surface. However, it diminishes at the external sphere surface.

4.2.3. Pressure-expansion response

The pressure-expansion curve is important to many engineering applications, such as indentation tests. For the spherical cavity expansion case, the pressure-expansion curves were obtained in terms of cavity pressure and the displacement at the external sphere wall, as shown in Fig. 9. The same set of parameters as in Section 4.2.2 have been used. Fig. 9(a) shows the pressure-expansion curve for both gradient theory and conventional theory at different frictional angles. The increase in frictional angle leads generally to a stronger expansion response, and the gradient-dependent response is largely stronger than that of the conventional theory, except when the plastic radius is approaching the external sphere wall in the case of large frictional angles. We have also investigated the effect of the internal length scale on the expansion response. Fig. 9(b) presents the results for the case of $\phi = 30°$, from which appreciable size effect has been observed. The use of larger values of internal length scale (relative to the cavity radius) generally produces a stronger pressure-expansion curve. However, the ultimate pressures at the fully plastic yielding stage appear to be roughly the same for all cases of ℓ. In addition,

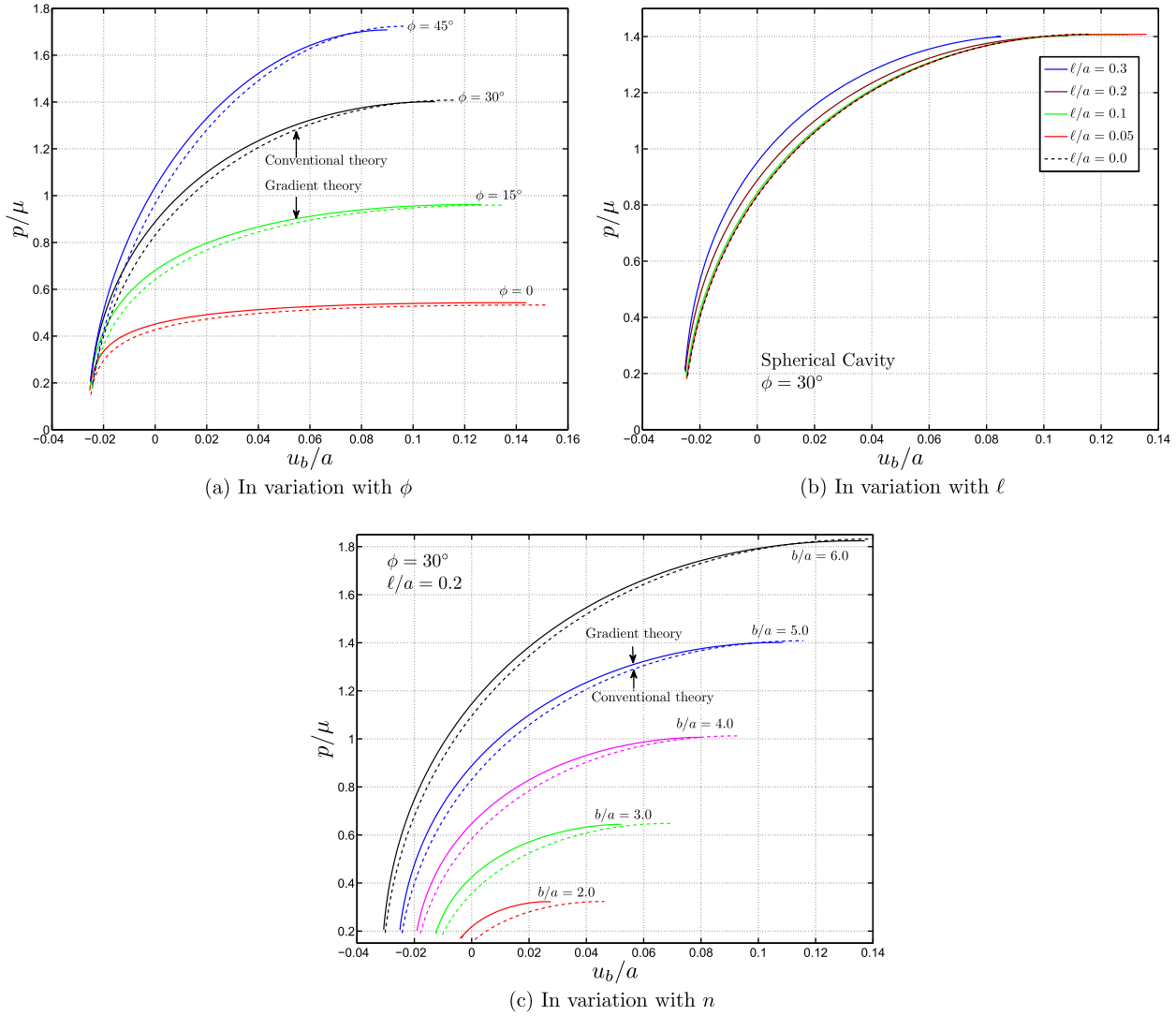

(a) In variation with ϕ

(b) In variation with ℓ

(c) In variation with n

Fig. 9. Variation of the pressure-expansion response of the hollow sphere (a) with frictional angle ϕ; (b) with the length scale ℓ; and (c) with the wall thickness ratio $n = b/a$.

the effect of the thickness ratio of the cavity wall on the pressure expansion response is significant, as is shown in Fig. 9(c). For the chosen case $\phi = 30^\circ$ and $\ell/a = 0.2$, five values of thickness ratio as shown in the figure have been used for the investigation. The thicker hollow spheres are found to show stronger response than the thin ones. Meanwhile, the gradient-dependent theory in general predicts stronger responses than the conventional theory for most part of the plastic expansion. The trend is reversed when the sphere enters the fully plastic stage.

5. Conclusion

A unified theory for both cylindrical and spherical cavity expansion problems has been reformulated to account for a special class of cohesive-frictional micromorphic media. By employing a strain-gradient theory, the governing equation and boundary conditions for one-dimensional cylindrical/spherical cavity expansion problem have been expressed in terms of generalized principal stresses. The Mohr–Coulomb criterion has been extended to address the cohesive-frictional behavior in the micromorphic media. In search for the elastic–plastic solution to the cavity expansion problem, robust numerical methods have been developed to solve the resulting two-point boundary value problem involving higher-order ODE which is slightly ill-conditioned in case of special parameter combination. The consistency and stability of these numerical methods are investigated and compared, and the one showing best performance has been chosen for the calculations. Using the theory and numerical procedure developed, the stress concentration at a cavity in an unbounded micromorphic medium subject to isotropic tension has been investigated. It is emphasized that, in quantifying the stress concentration, the generalized stress should serve as a more comprehensive measure rather than the conventional hoop stress alone. Meanwhile, the present study has found that the stress concentration is not necessarily always stronger than that predicted by the conventional theory, which is different from observations in some previous studies. It has also been demonstrated that, if the micromorphic properties of the material are considered, the cavity expansion of a hollow sphere/cylinder shows appreciable size effect. The frictional property also affects the elastic–plastic behavior considerably during the expansion of a cavity in a micromorphic material.

While the study has been motivated by the phenomenon of indentation size effect, emphasis in this paper has been placed on the aspects of theoretical formulation and numerical algorithms. Applications of the theory to the prediction ISE for various materials and other problems will be pursued in a future study.

Acknowledgments

This work was supported by the Research Grants Council of Hong Kong (under Project No. 623609). The author appreciates the comments made by Prof. S. Kyriakides and an anonymous reviewer which help improve the quality of the manuscript.

References

Abu Al-Rub, R., 2007. Prediction of micro- and nano indentation size effect from conical or pyramidal indentation. Mech. Mater. 39 (8), 787–802.
Ascher, U., Matthejj, R., Russell, R., 1995. Numerical Solution of Boundary Value Problems for Ordinary Differential Equations. SIAM (reprint of the first Prentice-Hall edition in 1988), Philadelphia, USA.
Bishop, R., Hill, R., Mott, N., 1945. The theory of indentation and hardness tests. Proc. Phys. Soc. 57 (3), 147–159.
Bleustein, J., 1966. Effects of micro-structure on the stress concentration at a spherical cavity. Int. J. Solids Struct. 2, 83–104.
Carter, J., Booker, J., Yeung, S., 1986. Cavity expansion in cohesive frictional soils. Géotechnique 36 (3), 349–353.
Chadwick, P., 1959. The quasi-static expansion of a spherical cavity in metals and ideal soils. Q. J. Mech. Appl. Math. 12, 52–71.
Chambon, R., Caillerie, D., El Hassan, N., 1998. One-dimensional localisation studied with a second grade model. Eur. J. Mech. – A/Solids 17 (4), 637–656.
Chambon, R., Caillerie, D., Matsushima, T., 2001. Plastic continuum with microstructure, local second gradient theories for geomaterials: localization studies. Int. J. Solids Struct. 38, 8503–8527.
Collin, F., Caillerie, D., Chambon, R., 2009. Analytical solutions for the thick-walled cylinder problem modeled with an isotropic elastic second gradient constitutive equation. Int. J. Solids Struct. 46 (22-23), 3927–3937.
Cook, T., Weitsman, Y., 1966. Strain-gradient effects around spherical inclusions and cavities. Int. J. Solids Struct. 2, 393–406.
Enright, W., Muir, P., 1993. A Runge–Kutta type boundary value ODE solver with defect control. Technical Report 267/93, Dept. Computer Science, Univ. Toronto, Toronto, Ont., Canada.
Eringen, C., 1999. Microcontinuum Field Theories. Foundations and Solids, vol. I. Springer-Verlag, Berlin.
Eshel, N., Rosenfeld, G., 1970. Effects of strain-gradient on the stress concentration at a cylindrical hole in a field of uniaxial tension. J. Eng. Math. 4 (2), 97–111.
Fleck, N., Hutchinson, J., 1997. Strain gradient plasticity. Adv. Appl. Mech. 33, 295–361.
Fleck, N., Hutchinson, J., 2001. A reformulation of strain gradient plasticity. J. Mech. Phys. Solids 49, 2245–2271.
Fleck, N., Muller, G., Ashby, M., Hutchinson, J., 1994. Strain gradient plasticity: theory and experiment. Acta Metal. Mater. 42, 475–487.
Gao, X., 2003. Strain gradient plasticity solution for an internally pressurized thick-walled spherical shell of an elastic-plastic material. Mech. Res. Commun. 30, 411–420.
Gao, X., Ma, H., 2010a. Solution of Eshelbys inclusion problem with a bounded domain and Eshelbys tensor for a spherical inclusion in a finite spherical matrix based on a simplified strain gradient elasticity theory. J. Mech. Phys. Solids 58, 779–797.
Gao, X., Ma, H., 2010b. Strain gradient solution for eshelby's ellipsoidal inclusion problem. Proc. R. Soc. A 466, 2425–2446.
Gao, H., Huang, Y., Nix, W., Hutchinson, J., 1999. Mechanism-based strain gradient plasticity–i. theory. J. Mech. Phys. Solids 47, 1239–1263.
Gao, X., Park, S., Ma, H., 2009. Analytical solution for a pressurized thick-walled spherical shell based on a simplified strain gradient elasticity theory. Math. Mech. Solids 14, 747–758.
Georgiadis, H., Vardoulakis, I., Lykotrafitis, G., 2000. Torsional surface waves in a gradient-elastic half-space. Wave Motion 31, 333–348.
Germain, P., 1973. The method of virtual power in continuum mechanics. part 2: microstructure. SIAM J. Appl. Math. 25, 556–575.
Gouldsone, A., Chollacoop, N., Dao, M., Li, J., Minor, A., Shen, Y., 2007. Indentation across size scales and disciplines: recent developments in experimentation and modeling. Acta Mater. 55, 4015–4039.
Hale, N., Moore, D., 2008. A sixth-order extension to the MATLAB package bvp4c of J. Kierzenka and L. Shampine. Technical Report NA-08/04, Oxford University Computing Laboratory, UK.
Hill, R., 1950. The Mathematical Theory of Plasticity. Oxford University Press, London.
Huang, Y., Zhang, F., Hwang, K., Nix, W., Pharr, G., Feng, G., 2006. A model of size effects in nano-indentation. J. Mech. Phys. Solids 54, 1668–1686.
Kelly, H., 1968. Numerical Methods for Two-Point Boundary-Value Problems. Blaisdell, London.
Kierzenka, J., Shampine, L., 2001. A BVP solver based on residual control and the MATLAB PSE. ACM Trans. Math. Softw. 27 (3), 299–316.
Mindlin, R., 1964. Micro-structure in linear elasticity. Arch. Ration. Mech. Anal. 16 (1), 51–78.
Mindlin, R., 1965. Second gradient of strain and surface-tension in linear elasticity. Int. J. Solids Struct. 1, 417–521.
Mühlhaus, H., Aifantis, E., 1991. A variational principal for gradient plasticity. Int. J. Solids Struct. 28, 845–857.
Nix, W., Gao, H., 1998. Indentation size effects in crystalline materials: a law for strain gradient plasticity. J. Mech. Phys. Solids 46 (3), 411–425.
Papanastasiou, P., Durban, D., 1997. Elastoplastic analysis of cylindrical cavity problems in geomaterials. Int. J. Numer. Anal. Meth. Geomech. 21, 133–149.
Shampine, L., Reichelt, M., 1997. The MATLAB ODE suite. SIAM J. Sci. Comput. (a publication of the Society for Industrial and Applied Mathematics) 18 (1), 1–22.
Stoer, J., Bulirsch, R., 2000. Introduction to Numerical Analysis, third ed. Springer, New York, USA.
Tabor, D., 1996. Indentation hardness: fifty years on – a personal view. Philos. Mag. A46, 617–628.
Yu, H., 2000. Cavity Expansion Methods in Geomechanics. Kluwer Academic Publisher.
Zhao, J., Pedroso, D., 2008. Strain gradient theory in orthogonal curvilinear coordinates. Int. J. Solids Struct. 45, 3507–3520.
Zhao, J., Sheng, D., Zhou, W., 2005. Shear banding analysis of geomaterials by strain gradient enhanced damage model. Int. J. Solids Struct. 42, 5335–5355.
Zhao, J., Sheng, D., Collins, I., 2006. Thermomechanical formulation of strain gradient plasticity for geomaterials. J. Mech. Mater. Struct. 1 (5), 837–863.
Zhao, J., Sheng, D., Sloan, S., 2007a. Cavity expansion of a gradient-dependent solid cylinder. Int. J. Solids Struct. 44, 4342–4368.
Zhao, J., Sheng, D., Sloan, S., Krabenhoft, K., 2007b. Limit theorems for gradient-dependent elastoplastic geomaterials. Int. J. Solids Struct. 44, 480–506.